Sensors & Actuators: B. Chemical 396 (2023) 134649

Contents lists available at ScienceDirect

Sensors and Actuators: B. Chemical

journal homepage: www.elsevier.com/locate/snb

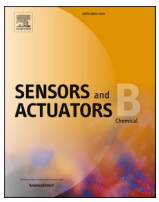

Synergistic enhancement of electrochemiluminescence through hybridization of α-Ge nanolayers and gold nanoparticles for highly sensitive detection of tyramine

Tamara Guerrero-Esteban [a], Borja L. Sánchez [d], Lucía Expósito [a], David Rodríguez-San-Miguel [d], Félix Zamora [d], Félix Pariente [a,b], Cristina Gutiérrez-Sánchez [a,b,*], Encarnación Lorenzo [a,b,c,*]

[a] Departamento de Química Analítica y Análisis Instrumental, Universidad Autónoma de Madrid, Madrid 28049, Spain
[b] Institute for Advanced Research in Chemical Sciences (IAdChem), Universidad Autónoma de Madrid, Ciudad Universitaria de Cantoblanco, Madrid 28049, Spain
[c] IMDEA-Nanociencia, Ciudad Universitaria de Cantoblanco, Madrid 28049, Spain
[d] Departamento de Química Inorgánica, Facultad de Ciencias and Condensed Matter Physics Center (IFIMAC), Universidad Autónoma de Madrid, Madrid 28049, Spain

ARTICLE INFO

Keywords:
Electrochemiluminescence sensing
Gold nanoparticles
α-Ge nanolayers
Tyramine
Sensor

ABSTRACT

This work presents a novel approach for detecting biogenic amine tyramine using a sensitive and disposable electrochemiluminescent sensor. The sensor is fabricated by modifying a screen-printed carbon electrode surface with two nanomaterials, α-Ge nanolayers and AuNP, which synergistically enhance the electrochemiluminescence response. The sensor was characterized using various techniques such as SEM-EDX, EIS, Raman, and AFM. The principle of the biosensor relays on the fact that tyramine molecule acts as an analyte and co-reactant, which interacts with the luminophore $[Ru(bpy)_3]^{2+}$ on the sensor surface. The proposed sensor shows a linear response to tyramine concentration, with a detection limit of 2.28 μM. The sensor successfully detected tyramine in avocado samples, demonstrating its potential for practical applications.

1. Introduction

Tyramine, 4-(2-aminoethyl)-phenol, is a monoamine that derives from the decarboxylation of the amino acid tyrosine. Tyrosine is a crucial component of many proteins and plays a significant role in several physiological processes. As a neuromodulator, tyramine can influence the activity of neurons in the brain while also acting as a precursor of the neurotransmitter octopamine. Overall, tyramine plays a crucial role in regulating the nervous system and has far-reaching implications for various bodily functions. Tyramine is also obtained by converting tyrosine into epinephrine, an active hormone produced internally in the adrenal gland. It can have toxic effects in high concentrations, causing allergic reactions, hypertension, or migraines [1]. In addition, human beings incorporate tyramine through our diet or through endogenous synthesis.

The tyramine levels found in different foods can vary depending on several factors, such as the availability of free tyrosine, the presence of microorganisms that produce tyramine, and the conditions that promote their growth. These conditions include factors such as salt concentration, temperature, and pH levels. As a result, foods that are high in tyramine, such as avocado or herring, or those that undergo fermentation during their production, contain significant amounts of this monoamine. It is essential to be aware of these variations in tyramine content, particularly for individuals who are sensitive to tyramine due to certain medical conditions or medication use [2]. Due to this, its sensitive and selective detection in foods is of great importance for preventing health risks and enhancing food safety [3].

Some methods developed for determining tyramine are based on high-performance thin-layer chromatography [4] and capillary electrophoresis [5]. Although these methods have high selectivity and low detection limit, they are expensive and require a long time in the treatment of samples and data analysis. There are also other alternatives for the detection of tyramine, such as fluorometric [6] or electrochemical determination through cyclic voltammetry and differential pulse voltammetry [7,8]. However, none of the current methods meet current demands, and it is still necessary to develop a simple, fast, and sensitive analytical method to determine tyramine.

Electrochemiluminescence (ECL) has advantages over other spectroscopic techniques besides providing accurate control of the time and position of the light-emitting reactions. The co-reactant based ECL needs

* Corresponding authors at: Departamento de Química Analítica y Análisis Instrumental, Universidad Autónoma de Madrid, Madrid 28049, Spain
E-mail addresses: cristina.gutierrezs@uam.es (C. Gutiérrez-Sánchez), encarnacion.lorenzo@uam.es (E. Lorenzo).

https://doi.org/10.1016/j.snb.2023.134649
Received 4 July 2023; Received in revised form 15 September 2023; Accepted 18 September 2023
Available online 19 September 2023

a substance that, when oxidized or reduced, will produce a reaction intermediate that will react with a luminophore to produce an excited species that can make light when they return to the ground state. A co-reactant must have various characteristics such as stability, solubility, high reaction rate, and electrochemically active. The most common co-reactants used with the luminophore $[Ru(bpy)_3]^{2+}$ complex are amines such as tri-n-propylamine [9] and taurine [10].

Tyramine belongs to the group of aromatic biogenic amines with a hydroxyl group and a primary amino group, so it could be a good ECL co-reactant, both capable of being easily oxidized and reduced. Thanks to this, it will react with a luminophore producing a ECL signal. Hence, it can be simultaneously co-reactant and analyte in a ECL based sensor. They have high sensitivity, low detection limit, good reproducibility and are fast and inexpensive, making them ideal for tyramine detection.

Recent investigations have shown that the intensity of ECL signals can be enhanced using nanomaterials. Therefore, different conductive nanomaterials, such as carbon nanotubes [11], carbon nanodots [12, 13], or gold nanoparticles (AuNP) [14] have been used to improve the ECL response. Recently, new nanomaterials such as nanocrystal semiconductors including SiO_2 [15], MoS_2 [16], ZnO [10] or quantum dots [17] have also been used with excellent results since the semiconductor nanoparticles can be electrochemically excited to generate the reduced or oxidized states of the nanoparticles, which can react with some co-reactants to produce ECL signals.

In this sense, alternative 2D nanomaterials, such as α-germanium nanolayers (α-GeNLs), which have interesting properties, exhibit band gaps that depend on their crystallographic directions and thickness. It should be noted that for the case of α-GeNLs, theoretical calculations point to an additional gap increase to 2.0 eV upon decreasing the thickness to 1 nm [18]. Therefore, the α-GeNLs could exhibit an excellent catalytic effect in the ECL system. These nanolayers have yet to be explored in ECL and could be excellent candidates for improving ECL performance. Hence, searching for new nanomaterials or combining several with suitable ECL activities has become an urgent challenge.

In this work, we have used α-germanium nanolayers (α-GeNLs), from isolated pristine nanolayers (NL), not α-Ge and nor α-Ge nanolayers, combined with AuNP to improve the sensitivity of a tyramine ECL-sensor. Pure α-germanium is exfoliated in a single step assisted by wet ball milling, enabling gram-scale fabrication of high-quality layers with large lateral dimensions and nanometer thicknesses. The result is the obtaining of nanometric 2D sheets. Screen-printed carbon electrodes have been modified with these sheets and AuNP. Combining the attractive functionalities of both nanomaterials, the ECL-based sensor platform shows enhanced synergistic properties. Tyramine acts simultaneously as co-reactant and analyte in the ECL system. The strategy developed is a new rapid method for Tyramine's selective and sensitive ECL-based determination. The applicability of the device has been demonstrated by the determination of the tyramine content in food samples.

2. Experimental

2.1. Chemical

Monobasic sodium phosphate (NaH_2PO_4), dibasic sodium phosphate dihydrate (Na_2HPO_3 2 H_2O), chlorauric acid ($HAuCl_4$ 3 H_2O), sodium citrate ($Na_3C_6H_5O_7$), tris(2,2′-bipyridine)ruthenium (II) dichloride hexahydrate ($[Ru(bpy)_3]Cl_2$ 6 H_2O), tyramine ($C_8H_{11}NO$), NaOH, HCl and compounds used in the preparation of the Britton-Robinson buffer solutions (phosphoric acid (H_3PO_4), acetic acid (CH_3COOH) and boric acid (H_3BO_3)) were obtained from Merck (Darmstadt, Germany).

The solutions were prepared using deionized water from a Millipore Milli-Q purification system.

The avocado samples have been acquired in a food establishment.

2.2. Instrumentation

The ECL experiments were carried out in an ECL cell with a Si-photodiode integrated and a potentiostat/galvanostat (±4 V DC potential range, ±40 mA maximum measurable current) supplied by Metrohm DropSens. Screen-printed carbon electrodes (SPCE) from the same company were used insides this cell. The protocol carried out for the ECL measurements is based on the addition of 60.0 μL of the solution to study the behavior of the working electrode modified with the nanomaterials. It is important that the working, pseudo-reference and auxiliary electrodes of the SPCE are completely covered. It should be noted that the solution to be studied must be free of bubbles since they can interfere with the measurement. Subsequently, the electrode confined in the cell was connected to the ECL equipment using a connector, and the measurement was started, carrying out three cyclic sweeps of potential between +0.00 to +1.10 V. The signals obtained show the intensity values of ECL and current intensity as a function of potential. All the experiments were carried out applying the conditions selected as optimal (2.00 mM $[Ru(bpy)_3]^{2+}$, the scan rate used was 30 mV/s and 0.1 M phosphate buffer pH 8.0). For electrochemical measurements a Metrohm-Autolab potentiostat PGSTAT 302 N was used. ECL responses have been normalized against control, that is, in the absence of analyte.

EIS experiments were performed in 0.1 M phosphate buffer, pH 7.0 in presence of 0.1 M KCl containing a mixture of 1.0 mM $K_3Fe(CN)_6$/1.0 mM $K_4Fe(CN)_6$. Impedance measurements were recorded in the range of frequency between 10^5 to 10^{-2} Hz, with a sinusoidal potential modulation of ±10 mV in amplitude superimposed onto the formal potential of the redox probe.

UV–Vis absorption spectra were performed on the PharmaSpec UV-1700 spectrometer (Shimadzu). Quartz cells with 1.0 cm optical path were used.

Zeta potential and DLS measurements were carried out with Zetasizer Nano ZS instrument (Malvern Instrument Ltd.).

Scanning electron microscopy (SEM) images were recorded using an FEI VERIOS 460 at 2.0 kV with beam deceleration. The samples were prepared simply by drop-casting 15 μL on Si surfaces with a layer of 250 nm of SiO_2 on the top (Si/SiO_2) over carbon double/sided tape. Transmission electron microscopy (TEM) images were obtained on a JEOL JEM 2100 FX TEM system with an accelerating voltage of 200 kV. The samples were prepared by drop-casting the dispersion to a honey carbon TEM grill (CF1.2/1.3–4 C-50).

Atomic force microscopy (AFM) images were taken with an Agilent 5500 microscope using a Cervantes Full mode AFM from Nanotec Electronica SL. WSxM software (www.wsxmsolutions.com) was employed both for data acquisition and image processing. AFM characterization has been made at air conditions, and Olympus OMCL-RC800PSA cantilevers (69 kHz and 71 kHz of resonance frequency) operate in air tapping mode. AFM samples were prepared on high-ordered pyrolytic graphite (HOPG).

Raman spectroscopy measurements were carried out using a confocal Raman microscope WITec alpha 300 R.

2.3. Procedures

2.3.1. Synthesis of α-GeNLs

The procedure of the synthesis of α-GeNLs was previously reported by us [18]. Therefore, the procedure involves a pre-grinding process of the α-Germanium crystal (Smart Elements Co, 99.999 % purity, polycrystalline) with an agate mortar resulting in so-called ground α-Ge. Afterward, the ground α-Ge powder was wet ball-milled: a 20 mL ball-milling reactor was charged with 600 mg of ground α-Ge, 30 stainless steel balls, and 2,5 mL of water/solvent mixture of 2-Propanol: H_2O (4:1 v/v). Then, the reactor was stirred for 60 min at 3000 rpm. After the wet ball-milling process, the wet powder was transferred to a 20 mL vial and dried under vacuum for 24 h at 60 °C. Subsequently, 10 mg of the dry powder of ball-milled α-Ge was shear mixed in a 20 mL vial

with 10 mL of a 2-Propanol/H_2O (4:1 v/v) mixture. The mixture was then dispersed with a shear-mixer device (IKA Ultra Turrax T25 digital) for 60 min at 25,000 rpm, using an ice bath as a chiller. Then, the resulting suspension of α-GeNLs was centrifuged for 3 min at 3000 rpm to homogenize the sample and discard unexfoliated material.

2.3.2. Synthesis of AuNP

The synthesis of AuNP was based on the following reduction reaction:

$$Na_3C_6H_5O_7 + HAuCl_4{\cdot}3\ H_2O \rightarrow AuNP$$

50.0 mL of 3.00 mM $HAuCl_4{\cdot}3\ H_2O$ solution was prepared, and the pH adjusted to 7.0 with 0.1 M NaOH. Subsequently, the $HAuCl_4{\cdot}3\ H_2O$ solution was transferred to a three-necked flask fitted with a magnet since the reaction was carried out under continuous stirring. Then, the $HAuCl_4{\cdot}3\ H_2O$ solution was heated to boil, reaching a temperature of 120 ºC and subsequently, 1.00 mL of $Na_3C_6H_5O$ was slowly added. It was left at reflux for 5 min, where a color change was observed in the mixture, turning from yellow to wine color; then, it was introduced into a Falcon tube and deposited in a cold-water bath to stop the reaction. It is worth mentioning that temperature is a fundamental factor for the synthesis to occur optimally and adequately, since in previous experiments carried out by the research group, it was observed that when the necessary temperature is not reached, could be formed of bulky aggregates of AuNP. Once the reaction was finished, the dialysis of the previously synthesized AuNP solution was carried out in a solution of 1200 mL of 1.00 mM citrate. The membrane used to carry out the dialysis has a size of MWCO:1kD. This allowed us to separate the reagents that had not reacted during the synthesis of the AuNP. Finally, the AuNP were stored at 4 ºC.

2.3.3. Modification of SPCE with α-GeNLs and AuNP

The modification of the SPCE was carried out in two stages, first, by spraying the α-GeNLs in isopropanol (SPCE/α-GeNLs) and next, by direct deposition by drop-casting of the AuNP (SPCE/α-GeNLs/AuNP). SPCE modification was performed on the working electrode by spraying α-GeNLs for 30 s. Once the surface was dry 25.0 μL of AuNP were added to the SPCE by drop-casting. For this, a volume of 5.00 μL was added five times; after each addition, it was left to dry in an oven at 38 ºC for 15 min. Following this procedure, a homogeneous platform was obtained on which the ECL measurements will subsequently be carried out.

2.3.4. Determination of tyramine in food samples

The applicability of the developed ECL-based sensor was demonstrated by analyzing the tyramine content in samples obtained from different avocados which a food establishment provided. 3.8286 g of avocado were weighed and introduced into 25.0 mL of 0.1 M phosphate buffer pH 8.0 on a beaker. The mixture was heated under continuous stirring for 90 min. Finally, the sample was filtered using a pleated filter to remove suspended particles. The filtrate was diluted 1:500 with 0.1 M phosphate buffer pH 8.0 and enriched with a known concentration of 50.0 μM tyramine to perform the determination by standard addition. The measurements were performed in an aqueous solution of 0.1 M phosphate buffer pH 8.0 containing the luminophore $[Ru(bpy)_3]^{2+}$ (2.00 mM). The potential was cycled between 0.00 V and + 1.10 V at 30 mV/s, and the ECL signal obtained was recorded.

3. Results and discussion

3.1. Development of the sensing platform (SPCE/α-GeNLs/AuNP)

In this work, we have developed a sensor based on ECL to determine tyramine (Ty). ECL reaction utilizes tyramine and $[Ru(bpy)_3]^{2+}$. In an oxidative-reduction mechanism, similar to the system of the tri-n-propylamine and $[Ru(bpy)_3]^{2+}$, the oxidation product of ty gives rise to an unstable highly reducing intermediate [9]. Upon electron transfer, the excited state of $[Ru(bpy)_3]^{2+}$ produces the emission observed.

From the CV (see Fig. S1), oxidation of Ty is carried out directly at the electrode surface. The electrochemically oxidation of Ty is a crucial step in the ECL process. The oxidation of Ty gives rise to highly reductive intermediate. This intermediate is the source of chemical energy to produce by reduction an excited state of the luminophore, which gives the ECL emission observed according to the following mechanism:

$$Ty \rightarrow {}^{\cdot+}Ty + e^-$$

$$[Ru(bpy)_3]^{3+} + {}^{\cdot+}Ty \rightarrow [Ru(bpy)_3]^{2+*} + \text{oxidized Ty product}$$

To improve the performance of the sensor, two nanomaterials of different natures, shapes, and sizes, α-GeNLs, and AuNP have been used to modify the electrode surface. One would expect that the combination of both nanomaterials provides new synergistic properties that are different from those already provided by both materials when used individually. AuNP show excellent electronic, sensing, optical, and catalytic properties.

3.1.1. Synthesis and characterization of α-GeNLs

The synthesis of α-GeNLs was performed as is described in the experimental section. The characterization was done by SEM and TEM to determine the morphology and size of the α-GeNLs. Additionally, AFM was carried out to study the topology and the thickness of the α-GeNLs. Finally, Raman spectroscopy was used to confirm the structural fingerprint of the α-GeNLs.

The SEM and TEM images (Fig. 1A and B) display the bidimensional features and crystallinity of the exfoliated α-GeNLs, with lateral dimensions between 300 and 400 nm. Moreover, AFM images (Fig. 1C) show the thickness of α-GeNLs ranging from 8 nm to 40 nm. Although the thickness has some grade of polydispersity, it confirms the bidimensionality of α-GeNLs. In addition, the AFM corroborated the lateral dimensions observed in SEM and TEM. Furthermore, Raman spectroscopy confirms the presence of peaks assigned to α-GeNLs (Fig. 1D and S9), specifically by the Raman peak at 300 cm^{-1} corresponding to the E_2 vibrational mode [18].

3.1.2. Synthesis and characterization of AuNP

AuNP were synthesized as described in the experimental section. It was characterized using different techniques such as UV-Vis absorption spectroscopy, DLS, and zeta potential.

The UV-Vis absorption spectrum (Fig. S4A) shows a band at 520 nm. Generally, AuNP present a single absorption band between 510 and 550 nm due to surface plasmon resonance and shows strong visible light absorption at 520 nm. This gives a bright red color that varies according to its size [19]. This result indicates the success of the synthesis of the AuNP.

The data obtained from the UV-Vis spectra (Fig. S4A) are supported by the particle size distributions studied using the DLS technique shown in Fig. S4B. A 1:10 dilution of AuNP shows two absorption maxima corresponding to two populations with different sizes of AuNP present in the solution, sizes between 0.8 and 32 nm.

Also, zeta potential measurements were made to obtain information on the magnitude of attraction or repulsion between the particles that are in suspension, depending on the charge. Regarding the Zeta potential study, the spectrum (Fig. S4C) shows two maxima, –48.0 mV and –36.7 mV. These values indicate that the synthesized AuNP have a negative surface potential, probably because the citrate present on their surface is used to stabilize them [20].

3.2. Nanostructuring of SPCE with α-GeNLs/AuNP

The SPCE was nanostructured by adding α-GeNLs and AuNP as described in the experimental section. Different volumes of AuNP (SPCE/AuNP) were deposited directly on the electrode surface by drop-

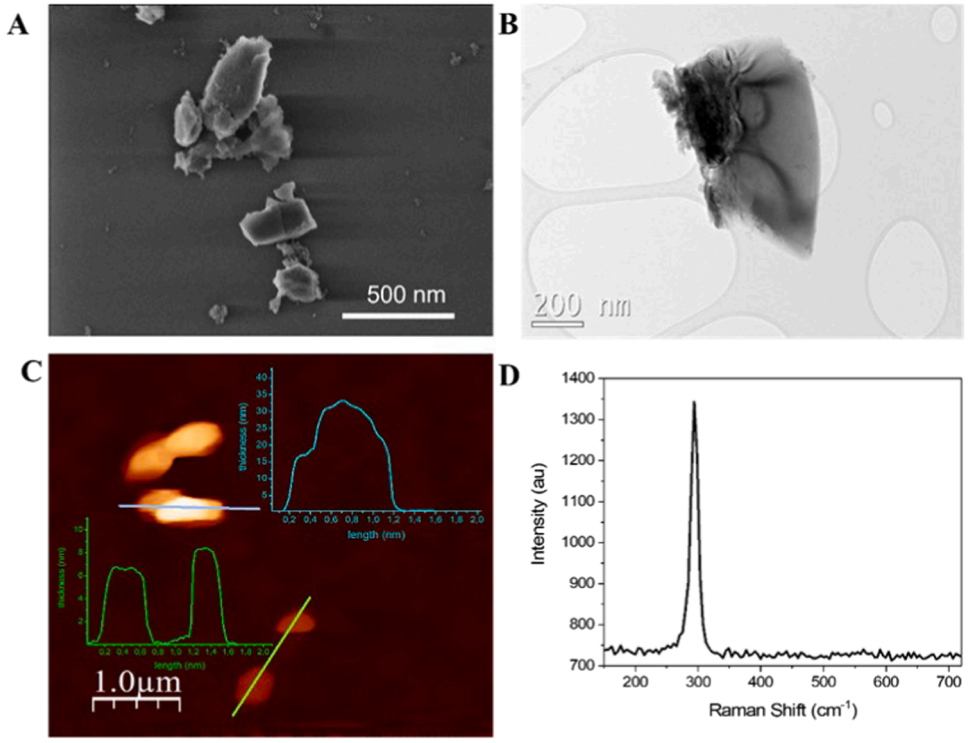

Fig. 1. A. SEM image and B. TEM image of the exfoliated α-GeNLs. C. AFM image and profiles of the α-GeNLs. D. Raman peak at 300 cm^{-1} confirms it is α-GeNLs, specifically 300 cm^{-1}, corresponding to the E_2 vibrational mode.

casting. After modifying the electrode, to verify the presence of gold on the SPCE associated with AuNP, its cyclic voltamperometric response (Fig. S5) was recorded between + 0.00 and + 1.30 V at 100 mV/s in 0.1 M H_2SO_4. Fig. S5A shows typical redox signals associated with gold. The intensity of the redox peaks increases as the volume of AuNP deposited on the electrode increases, indicating that more AuNP were immobilized on the SPCE surface. Likewise, the voltammogram corresponding to the unmodified SPCE does not present any signal produced by oxidation or reduction processes since there is no presence of any gold oxide associated with the AuNP.

Once it was verified that the SPCE was correctly modified with the AuNP, an ECL study was carried out at these electrodes in the presence of 2.00 mM $[Ru(bpy)_3]^{2+}$, which acts as a luminophore. As shown in Fig. S5B, as the amount of AuNP on the SPCE increases, the ECL response increases up to a volume of 25.0 μL. No significant differences in ECL signal were observed between 25.0 and 30.0 μL. The presence of AuNP increases the relative electrode surface area and improves the conductivity, improving the ECL signal (Fig. 2A). The excited state of the luminophore would excite the surface plasmon resonance of AuNP, which in turn induces an increase of the near electromagnetic field of AuNP. This increase could enhance the ECL emission [21,22].

It has been described, in the introduction section, that the use of semiconductors such as ZnO nanowires [10], or quantum dots [23], or MoS_2 [24] has shown an improvement in the performance of the ECL platforms, in particular when semiconductors are combined with other materials or nanomaterials due to the synergistic effects. This improvement is probably due to recombination of excitons and the defects in the nanoparticles, of the semiconductor nanomaterials. Also, semiconductor nanoparticles can be electrochemically excited to generate the reduced or oxidized states of the nanoparticles, which can react with the co-reactants to enhance the electrochemiluminescent response. Based on these previous results, after modification with AuNP, the SPCE electrode was modified with the α-GeNLs by spraying a dispersion of α-GeNLs (1.00 mg/mL) (SPCE/α-GeNLs), and the ECL response was recorded in 0.1 M phosphate buffer pH 8.0 solution containing 2.00 mM $[Ru(bpy)_3]^{2+}$. As a comparison, the electrode was also

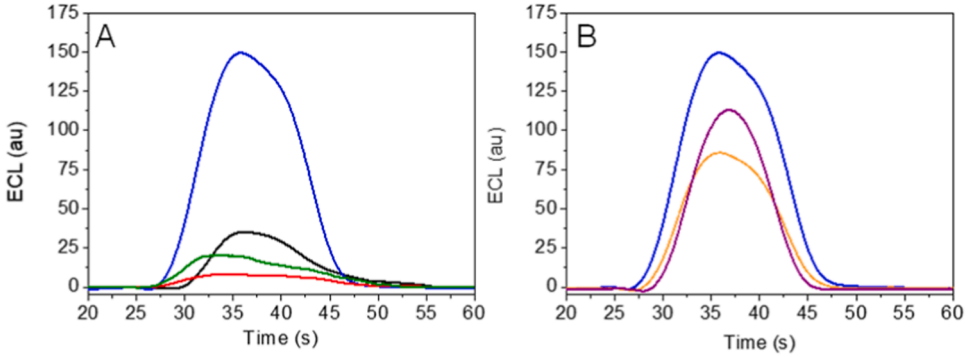

Fig. 2. A. ECL response at SPCE (red line), SPCE/α-GeNLs (black line), SPCEAuNP (green line), and SPCE/α-GeNLs/AuNP (blue line). B. ECL response at SPCE was modified with different spray times using α-GeNLs: 30 s (blue line), 1 min (purple line), 2 min (orange line). The ECL measurements were done in 0.1 M phosphate buffer pH 8.0 solution containing 2.00 mM $[Ru(bpy)_3]^{2+}$ at 30 mV/s scan rate.

modified only with the same α-GeNLs dispersion following the same procedure and the ECL response were recorded at the same conditions. Fig. 2A shows that the electrode modified with α-GeNLs and AuNP (SPCE/α-GeNLs/AuNP) shows the highest response. We can observe that the presence of both nanomaterials results in an increase in the ECL signal of up to 5 times. This behavior has also been observed with other nanomaterials, when a combination of them with different properties have been employed, as is our case. In fact, the response of ECL platforms based on quantum dots is improved with the addition of metallic nanoparticles such as silver nanoparticles [25]. This improvement also occurred using other metallic nanostructures, such as gold nanocages [26]. These results confirm that the combination of nanomaterials shows excellent ECL properties due to the synergistic effects. It has been described that AuNP are frequently used in Surface Plasmon Resonance (SPR), SPR Enhanced Raman Spectroscopy due to the strong near-field electromagnetic increase derived from resonance. In particular, it has been described that SPR, SERS and SPR enhanced fluorescence by this effect and recently ECL [27–30]. When AuNP are combined with the presence of a semiconductor, a greater increase in the local electromagnetic field could occur, which produces an increase in the radiative decay rate of the Γm and Förster energy transfer, which could increase the intensity of ECL [31].

Following this, the coating of α-GeNLs on the SPCE/AuNP was optimized. For this, the spray time of the α-GeNLs dispersion was varied. Fig. 2B shows that as the α-GeNLs dispersion spray time increases, the amount of α-GeNLs on the electrode surface increases, and ECL intensity decreases. This could be due to light scattering occurring, reducing the ECL intensity. This behavior has also been observed with semiconductors such as ZnO [10]. Based on the best ECL values obtained, the selected time to spray the α-GeNLs dispersion was 30 s. This value was selected because it provides a higher ECL signal and, in addition, a lower amount of α-GeNLs is required.

From the optimization studies, we can conclude that the electrode that offered a more significant ECL response was prepared using 30 s of α-GeNLs and 25.0 μL of AuNP. Surface modification of the SPCE was performed, as mentioned above in the experimental procedure, using spray and drop-casting techniques, respectively, to obtain a homogeneous surface. This modification will be used later in the preparation of all platforms.

3.3. Characterization of the modified SPCE/α-GeNLs/AuNP

To fabricate reproducible devices, we have carried out an exhaustive characterization of each development step by different techniques such as SEM-EDX, EIS, Raman, and AFM.

EDX-analysis was used to characterize the surface and thus verify the correct nanostructuring of the platform. The EDX-analysis of the bare SPCE unmodified electrode (Fig. S6A) shows significant signs of carbon. The spectra corresponding to the SPCE/AuNP, SPCE/α-GeNLs, and SPCE/α-GeNLs/AuNP (Fig. S6B, 6C and 6D) show signals associated with the nanomaterials used for their modification, such as gold, germanium, and gold/germanium, respectively. It is worth mentioning that the spectrum of SPCE/AuNP presents a sodium signal from the AuNP synthesis process. All these results confirm the presence of gold and germanium atoms from the nanomaterials used in the SPCE modification and, therefore, the success of the process.

SEM images were also obtained for bare and modified electrodes (Inset of Fig. S6) and the analysis of each element can be seen in more detail in Fig. S6. These results are corroborated by the high-resolution SEM images and the analysis of each element shown in a different color. In Fig. S2, S3, and S7 each element is shown individually.

EIS is an important experimental electrochemical technique that identifies phenomena associated with kinetic and mass transport constraints. In the present work it was employed to study the interfacial properties of the developed electrode surfaces. The measurements were recorded in a frequency range from 10^5 to 10^{-2} Hz, with a modulation of the sinusoidal potential of ± 10 mV amplitude superimposed on the formal potential of the redox probe used ($K_3Fe(CN)_6/K_4Fe(CN)_6$). Fig. S8 shows the Nyquist plots obtained at SPCE, SPCE/AuNP, SPCE/α-GeNLs, and SPCE/α-GeNLs/AuNP. After the modification of the SPCE with the two nanomaterials used, a decrease in the diameter of the semicircle is observed, which is related to the resistance to charge transfer. The larger diameter of the semicircle, the greater the resistance to charge transfer and, therefore, the lower the conductivity of the electrode. The SPCE/α-GeNLs/AuNP shows a lower resistance. In fact, the value of charge transfer resistance greatly decreased from 450 Ω measured at bare SPCE to 10 Ω. This result agrees well with the higher conductivity due to the presence of AuNP, since being a metallic nanomaterial, have conductive properties. A very similar charge transfer resistance value was obtained in the case of the electrode modified only with AuNP. It can also be seen how when adding α-GeNLs, the conductivity decreases compared to the unmodified SPCE, but increases compared to SPCE/AuNP since α-GeNLs is a semiconductor nanomaterial. All these results indicate an improvement in the conductivity of the electrode surface, in addition to confirm the correct modification of the SPCE with the nanomaterials.

To further characterize the sensing ECL platform and check the correct nanostructuring of the SPCE/α-GeNLs, Raman spectroscopy was used, obtaining the corresponding spectrum (Fig. S9A). Optical microscope images corresponding to the SPCE/α-Ge were also obtained (Fig. S9B), where a more excellent brightness produced by the presence of α-GeNLs is observed compared to the image obtained for a bare SPCE (Fig. S9C). Measurements were made using a 50 × objective, an excitation wavelength laser of 532 nm, with a power of 200 mW and 20 stacks. In the spectrum, a band centered around 300 cm^{-1} corresponding to the exfoliated α-GeNLs is observed, thus reaffirming the correct nanostructuring of the SPCE with the α-GeNLs [18]. Bibliographic data provide that the band observed in the Raman spectrum is related to α-GeNLs [32]. No significant differences were observed between SPCE/α-GeNLs and SPCE/α-GeNLs/AuNP (Data not shown).C.

B.

Additional optical microscopy and Raman spectroscopy were performed to obtain a Raman map (Fig. 3). Raman spectra were recorded using an excitation laser of 532 nm and a grating of 600 g/mm (spectral center at 2040 cm^{-1}). The Raman map was then generated by integrating the counts of the characteristic. Optical microscope images corresponding to the SPCE/α-GeNLs were also shown (Fig. 3), where a greater brightness produced by the presence of α-GeNLs is observed, compared to the image obtained for a bare SPCE (Fig. S9C). Measurements were made using a 50x objective, an excitation wavelength laser of 532 nm, with a power of 200 mW and 20 stacks. In the Raman spectrum (Fig. 3C), a band centered around 300 cm^{-1} is observed, corresponding to the E_2 vibrational mode of the exfoliated α- Ge, thus reaffirming the correct nanostructuring of the SPCE with the α-GeNLs [18]. In addition, the Raman spectrum confirms that α-GeNLs are not oxidated due to there are not any peak at 440 or 700 cm^{-1} associated to different allotropies of germanium oxides. Bibliographic data confirm that the band observed in the Raman spectrum is related to α-GeNLs [32]. No significant differences were observed between SPCE/α-GeNLs and SPCE/α-GeNLs/AuNP (Data not shown).

To obtain morphological information and confirm the correct modification of electrodes with α-GeNLs and AuNP, they were subjected to AFM. Fig. S10 of information shows topographical AFM images of a HOPG surface modified with α-GeNLs and AuNP as described in procedures. It can be observed that the surface is partially covered with an α-GeNLs film, and spherical structures associated with AuNP appear on it.

3.4. Optimization of experimental variables

In order to obtain the best ECL response of the SPCE/α-GeNLs/AuNP platform for the determination of tyramine, the experimental variables such as the concentration of $[Ru(bpy)_3]^{2+}$, scan rate and the pH of the

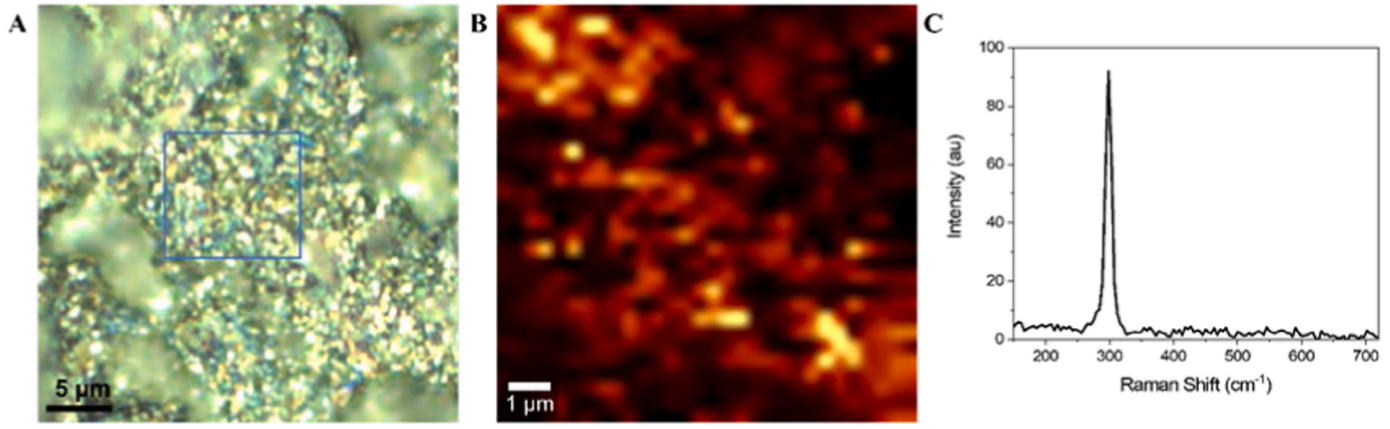

Fig. 3. (A) Optical image of SPCE/α-GeNLs, the squared area is where the Raman mapping has been done. (B) Raman mapping of SPCE/α-GeNLs showing the E_2 vibrational mode of α-GeNLs at 300 cm^{-1} and (C) Raman average spectrum of α-GeNLs at Raman mapping of SPCE/α-GeNLs.

buffer solution were optimized (Fig. S11).

Initially, the concentration of the luminophore $[Ru(bpy)_3]^{2+}$ varied between 1.00 mM and 4.00 mM. The ECL signal increases considerably on increasing the concentration from 1.00 mM to 2.00 mM, then decreases and stabilizes until reaching a pseudo-plate (Fig. S11A).

Also, the ECL signal obtained when the scan rate is varied, in a range between 10 mV/s and 40 mV/s, was studied (Fig. S11B). The ECL intensity increases until a maximum of 30 mV/s, after which there is a sharp decrease when it goes to 40 mV/s.

Finally, we studied the pH effect on the ECL reponse. Different measurements were performed at pH ranging from 6.0 to 9.0. The ECL signal increases as the pH of the solution becomes more alkaline, up to a maximum of 8.0, from which a decrease is observed (Fig. S11C). Ty is involved in an acid-base balance with two different ionic forms in aqueous solution ($pK_a = 9.74$). The large pH influence for ECL observed is consistent with deprotonation of the radical cation of Ty as a critical step in forming the strong reducing agent. The ECL intensity decreases when the pH is not basic enough to deprotonate the Ty radical cation. Since the pH range is more acidic than the pKa of Ty, we believe the acidity of Ty radical cation and not the basicity of Ty plays a crucial role in the pH influence on ECL. This behavior has been observed in other molecules containing amino groups, such as taurine [10], glyphosate [33], and tri-n-propylamine [9].

After carrying out the study of the optimization of the experimental variables, it is concluded that the optimal conditions are a concentration of 2.00 mM $[Ru(bpy)_3]^{2+}$, a pH of 8.0, and a scan rate of 30 mV/s since all of them give the maximum ECL signal.

3.5. Analytical performance of tyramine ECL-sensor

Once all the experimental conditions were established, the response of the ECL-based sensor was evaluated to different concentrations of tyramine. Solutions containing 2.00 mM $[Ru(bpy)_3]^{2+}$ and increasing concentrations of tyramine in 0.1 M phosphate buffer at pH 8.0 were prepared. A cyclic potential sweep was applied from + 0.00 V to + 1.10 V at 30 mV/s.

Fig. 4A shows that the ECL-based sensor response increases as the tyramine concentration increases, revealing that it acts as co-reactant and analyte simultaneously. The calibration curve obtained demonstrates the linear dependence ($R^2 = 0.997$) between the ECL signal and the tyramine concentration for a concentration range from 10.0 μM to 250 μM, with a sensitivity of 0.37 ± 0.01 a.u . μM^{-1}, calculated from the slope of the calibration curve.

From these linear fits, the limits of detection (LD) and quantification (LQ) were calculated according to the criterion X_{blank}-3S_b/m and X_{blank}-10 S_b/m, respectively, where S_b is the standard deviation of the blank signal, and m is the slope of the calibration plot. LD and LQ of 2.28 μM and 7.60 μM, respectively, were obtained. The relative standard deviation (RSD) obtained was 2.37 %, showing the excellent reproducibility of the sensor.

The analytical parameters of the sensor developed have been compared with those of other methods employed to determine tyramine (Table 1). The LD reached with the present method is relatively low. Although previous work based on ECL detection technique got a lower LD, it requires the use of coupled capillary electrophoresis. The advantage of the sensor developed in the present work is that it is most straightforward and affordable and allows determining tyramine directly in the sample. Considering all the advantages mentioned above, it can be concluded that the ECL-based sensor developed has shown to be a competitive method for determining tyramine.

The stability and durability of the developed platform were also evaluated. Regarding the durability of the modified SPCE, ten

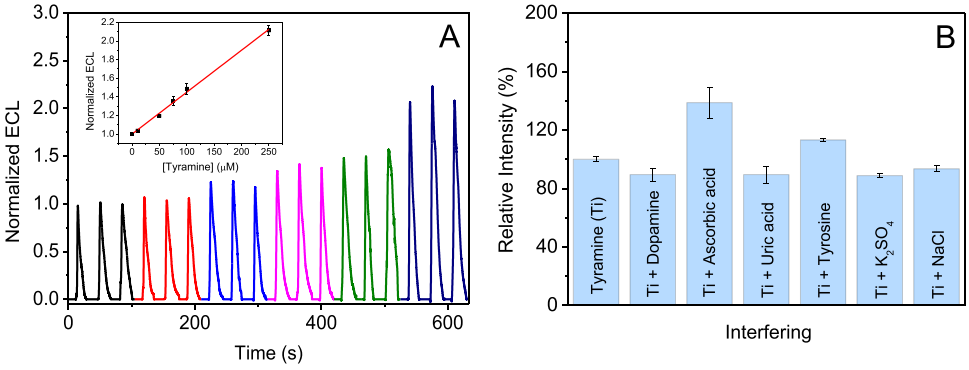

Fig. 4. (A) ECL sensor responses as a function of increasing tyramine concentration at SPCE/α-GeNLs/AuNP. Each point corresponds to the mean of three measurements, each of them carried out with three different electrodes. Inset: Calibration curve. (B) Relative intensity for 50.0 μM tyramine (Ti) in the absence or presence of potentially interfering compounds. The ECL measurements were carried out in 0.1 M phosphate buffer pH 8.0 solution containing 2.00 mM $[Ru(bpy)_3]^{2+}$ at 30 mV/s scan rate.

Table 1
Comparative table of different methods for the determination of tyramine.

Detection technique	Modified electrode configuration	Range / μM	LD / μM	Ref.
DPV EIS	molecularly imprinted polymer/Pt disk electrode	290–2640	159 168	[34]
Potentiometry	ion-exchanger/ plasticizer/PVC/glassy carbon electrode	77.3–10000	57,6	[35]
DPV	functionalized multi-walled carbon nanotubes/glassy carbon electrode	1–17 / 17–85	0.42	[36]
DPV	poly(3-methylthiophene)/Pt electrode	4.40–14000	1.32	[37]
Capillary electrophoresis coupled with ECL	-	0.73–729	0.087	[38]
ECL	SPCE/α-GeNLs/AuNP	7.60–250	2.28	This work

DPV: Differential Pulse Voltammetry; EIS: Electrochemical Impedance Spectroscopy; PVC: high molecular weight polyvinyl chloride

consecutive measurements were made in the presence of 2.00 mM $[Ru(bpy)_3]^{2+}$ and 50.0 μM tyramine. As seen in Fig. S12A, the ECL signal progressively decreases until the fifth cycle and subsequently a pseudoplate is reached. The recorded signals of the tyramine sensor kept about 87 % of the initial value.

The stability of the platform was evaluated in the presence of 2.00 mM $[Ru(bpy)_3]^{2+}$ and 50.0 μM tyramine for 16 days. The results (Fig. S12B) confirm the sensor response is stable for at least ten days, then there is a decrease on the sixteenth day.

One of the key aspects to consider sensors for any analytical application is the effect of possible interfering compounds that may be present in the samples. For this reason, the selectivity of the proposed sensor was tested against various potentially interfering compounds. The interferents studied were dopamine, ascorbic acid, uric acid, tyrosine, potassium sulfate (K_2SO_4), and sodium chloride (NaCl). These compounds were selected because they are structurally similar or coexist with tyramine [39]. As detailed in the introduction section, the compounds that have amines or alcohols in their structure can act as co-reactants in ECL in the presence of $[Ru(bpy)_3]^{2+}$. Therefore, it may cause interference. The selectivity of the sensor was evaluated by recording its response to tyramine in the presence of the potentially interfering compounds, all at a concentration of 50.0 μM.

The only substance that showed a noticeable interference effect is ascorbic acid. Ascorbic acid is a common interferant because it has a critical reducing effect.

In contrast, the rest of the substances studied do not show significant changes in the ECL response.

3.6. Determination of tyramine in food samples

The developed ECL-based sensor was applied to direct determination of tyramine in an avocado. Sample pretreatment is detailed in procedures.

The intensity of ECL provided by samples from three avocados spiked with 50.0 μM tyramine and in the presence of 2.00 mM $[Ru(bpy)_3]^{2+}$ was measured. From the signal ratio between the sample and the sample fortified with 50 μM, it has been found a tyramine concentration of (0.3503 ± 0.05) grams (for three determinations) in 3.8286 g of avocado.

The ECL signal for the fortified sample corresponds to 51.7 μM of tyramine giving a recovery of (103 ± 5) % (n = 3). Therefore, it can be concluded that the developed ECL based sensor can be used for the determination of tyramine directly in food samples, without the need of any previous separation step. In addition, the fabrication of this sensors proposed can also be applied to develop other ECL based sensors for the detection of trace levels of different analytes of interest.

4. Conclusions

This study builds and evaluates a straightforward nanostructured electrochemical platform to create a highly selective and efficient ECL-based sensor for detecting tyramine. By combining two nanomaterials, α-GeNLs and AuNP, the sensor platform was nanostructured, resulting in a significant increase in the ECL signal. Tyramine acts as both an analyte and co-reactant in the ECL system. The resulting throwaway sensor has a low detection limit of 2.28 μM, high selectivity, reproducibility, and stability.

Finally, the applicability of the sensor was demonstrated by using it to determine tyramine directly in avocado samples, indicating its potential for food sample analysis.

CRediT authorship contribution statement

T. G-E.: Investigation. **B.L.S.:** Investigation. **L. E.**: Investigation. **D. R-S. M.**: Investigation. **F.Z.:** Writing, Funding Acquisition. **F. P.**: Conceptualization. **C. G-S.**: Conceptualization, Supervision, Writing, Funding Acquisition., **E. L.**: Conceptualization, Supervision, Writing, Funding Acquisition.

Declaration of Competing Interest

The authors declare that they have no known competing financial interests or personal relationships that could have appeared to influence the work reported in this paper.

Data Availability

Data will be made available on request.

Acknowledgments

This work has been supported the Comunidad Autónoma de Madrid (2021-5A/BIO-20943 Talent Attraction Project, SI3/PJI/2021-00341 and S2018/NMT-4349 TRANSNANOAVANSENS-CM Program) and by the Spanish Ministerio de Ciencia e Innovación (PID2020-116728RB-I00, PDC2021-120782-C21, PID2019-106268GB-C32 and TED2021-129738B-I00). This work has also been supported by the Spanish MINECO (PID2019-106268GB-C32, CEX2018-000805-M and PDC2021-120782-C21). We acknowledge the support from the "(MAD2D-CM)-UAM" project funded by Comunidad de Madrid, by the Recovery, Transformation and Resilience Plan, and by NextGenerationEU from the European Union.

Appendix A. Supporting information

Supplementary data associated with this article can be found in the online version at doi:10.1016/j.snb.2023.134649.

References

[1] S. Dhakal, I. Macreadie, Tyramine and amyloid beta 42: a toxic synergy, Biomedicines 8 (2020) 145.
[2] G. Andersen, P. Marcinek, N. Sulzinger, P. Schieberle, D. Krautwurst, Food sources and biomolecular targets of tyramine, Nutr. Rev. 77 (2018) 107–115, https://doi.org/10.1093/nutrit/nuy036.
[3] K. Kaewjua, W. Siangproh, A novel tyramine sensing-based polymeric L-histidine film-coated screen-printed graphene electrode: capability for practical applications, Electrochim. Acta 419 (2022), 140388, https://doi.org/10.1016/j.electacta.2022.140388.

[4] A. Romano, H. Klebanowski, S. La Guerche, L. Beneduce, G. Spano, M.-L. Murat, P. Lucas, Determination of biogenic amines in wine by thin-layer chromatography/densitometry, Food Chem. 135 (2012) 1392–1396, https://doi.org/10.1016/j.foodchem.2012.06.022.
[5] W. Li, Y. Pan, Y. Liu, X. Zhang, J. Ye, Q. Chu, Simultaneous determination of eight typical biogenic amines by CZE with capacitively coupled contactless conductivity detection, Chromatographia 77 (2014) 287–292, https://doi.org/10.1007/s10337-013-2595-3.
[6] Y. Chen, F. Fan, G. Fang, Q. Deng, S. Wang, Fluorometric determination of tyramine by molecularly imprinted upconversion fluorescence test strip, Microchim. Acta 187 (2020), 573, https://doi.org/10.1007/s00604-020-04554-7.
[7] M.Z.H. Khan, X. Liu, J. Zhu, F. Ma, W. Hu, X. Liu, Electrochemical detection of tyramine with ITO/APTES/ErGO electrode and its application in real sample analysis, Biosens. Bioelectron. 108 (2018) 76–81, https://doi.org/10.1016/j.bios.2018.02.042.
[8] L.D. Chakkarapani, M. Brandl, Highly sensitive electrochemical detection of tyramine using a poly(toluidine blue)-modified carbon screen-printed electrode, IEEE Sens. J. 22 (2022) 2974–2983, https://doi.org/10.1109/jsen.2021.3109660.
[9] J.K. Leland, M.J. Powell, Electrogenerated chemiluminescence: an oxidative-reduction type ECL reaction sequence using tripropyl amine, J. Electrochem. Soc. 137 (1990) 3127–3131, https://doi.org/10.1149/1.2086171.
[10] T. Guerrero-Esteban, C. Gutiérrez-Sánchez, M. Revenga-Parra, J.L. Pau, F. Pariente, E. Lorenzo, Enhanced electrochemiluminescence by ZnO nanowires for taurine determination, Talanta 204 (2019) 63–69, https://doi.org/10.1016/j.talanta.2019.05.090.
[11] R.-F. Huang, L.-T. Wang, Q.-Q. Gai, D.-M. Wang, L. Qian, DNA-mediated assembly of carbon nanotubes for enhancing electrochemiluminescence and its application, Sens. Actuators B: Chem. 256 (2018) 953–961, https://doi.org/10.1016/j.snb.2017.10.033.
[12] T. Guerrero-Esteban, C. Gutiérrez-Sánchez, E. Martínez-Periñán, M. Revenga-Parra, F. Pariente, E. Lorenzo, Sensitive glyphosate electrochemiluminescence immunosensor based on electrografted carbon nanodots, Sens. Actuators B: Chem. 330 (2021), 129389, https://doi.org/10.1016/j.snb.2020.129389.
[13] T. Guerrero-Esteban, C. Gutiérrez-Sánchez, A.M. Villa-Manso, M. Revenga-Parra, F. Pariente, E. Lorenzo, Sensitive SARS-CoV-2 detection in wastewaters using a carbon nanodot-amplified electrochemiluminescence immunosensor, Talanta 247 (2022), 123543, https://doi.org/10.1016/j.talanta.2022.123543.
[14] T.T. Bezuneh, T.H. Fereja, S.A. Kitte, H. Li, Y. Jin, Gold nanoparticle-based signal amplified electrochemiluminescence for biosensing applications, Talanta 248 (2022), 123611, https://doi.org/10.1016/j.talanta.2022.123611.
[15] G.B. Grad, E.R. González, J. Torres-Díaz, E.V. Bonzi, A DFT study of ZnO, Al2O3 and SiO2; combining X-ray spectroscopy, chemical bonding and Wannier functions, J. Phys. Chem. Solids 168 (2022), 110788, https://doi.org/10.1016/j.jpcs.2022.110788.
[16] Y. Liu, Y. Nie, M. Wang, Q. Zhang, Q. Ma, Distance-dependent plasmon-enhanced electrochemiluminescence biosensor based on MoS2 nanosheets, Biosens. Bioelectron. 148 (2020), 111823, https://doi.org/10.1016/j.bios.2019.111823.
[17] X. Chen, Y. Liu, Q. Ma, Recent advances in quantum dot-based electrochemiluminescence sensors, J. Mater. Chem. C 6 (2018) 942–959, https://doi.org/10.1039/c7tc05474b.
[18] C. Gibaja, D. Rodríguez-San-Miguel, W.S. Paz, I. Torres, E. Salagre, P. Segovia, E. G. Michel, M. Assebban, P. Ares, D. Hernández-Maldonado, Q. Ramasse, G. Abellán, J. Gómez-Herrero, M. Varela, J.J. Palacios, F. Zamora, Exfoliation of alpha-germanium: a covalent diamond-like structure, Adv. Mater. 33 (2021), 2006826, https://doi.org/10.1002/adma.202006826.
[19] H.N. Verma, P. Singh, R.M. Chavan, Gold nanoparticle: synthesis and characterization, Vet. World 7 (2014) 72–77, https://doi.org/10.14202/vetworld.2014.72-77.
[20] C.H. Munro, W.E. Smith, M. Garner, J. Clarkson, P.C. White, Characterization of the surface of a citrate-reduced colloid optimized for use as a substrate for surface-enhanced resonance Raman scattering, Langmuir 11 (1995) 3712–3720, https://doi.org/10.1021/la00010a021.
[21] D. Wang, L. Guo, R. Huang, B. Qiu, Z. Lin, G. Chen, Surface enhanced electrochemiluminescence of Ru(bpy)32+, Sci. Rep. 5 (2015), 7954 https://doi.org/10.1038/srep07954.
[22] J. Zhang, Z. Gryczynski, J.R. Lakowicz, First observation of surface plasmon-coupled electrochemiluminescence, Chem. Phys. Lett. 393 (2004) 483–487, https://doi.org/10.1016/j.cplett.2004.06.050.
[23] X.-L. Liang, N. Bao, X. Luo, S.-N. Ding, CdZnTeS quantum dots based electrochemiluminescent image immunoanalysis, Biosens. Bioelectron. 117 (2018) 145–152, https://doi.org/10.1016/j.bios.2018.06.006.
[24] Y. Zhang, H. Yin, C. Jia, Y. Dong, H. Ding, X. Chu, Electrogenerated chemiluminescence of Ru(bpy)32+ at MoS2 nanosheets modified electrode and its application in the sensitive detection of dopamine, Spectrochim. Acta Part A: Mol. Biomol. Spectrosc. 240 (2020), 118607, https://doi.org/10.1016/j.saa.2020.118607.
[25] F. Liu, S. Ge, M. Su, X. Song, M. Yan, J. Yu, Electrochemiluminescence device for in-situ and accurate determination of CA153 at the MCF-7 cell surface based on graphene quantum dots loaded surface villous Au nanocage, Biosens. Bioelectron. 71 (2015) 286–293, https://doi.org/10.1016/j.bios.2015.04.051.
[26] P. Zhang, Y. Zhuo, Y. Chang, R. Yuan, Y. Chai, Electrochemiluminescent graphene quantum dots as a sensing platform: a dual amplification for MicroRNA assay, Anal. Chem. 87 (2015) 10385–10391, https://doi.org/10.1021/acs.analchem.5b02495.
[27] J. Wang, Y. Shan, W.-W. Zhao, J.-J. Xu, H.-Y. Chen, Gold nanoparticle enhanced electrochemiluminescence of CdS thin films for ultrasensitive thrombin detection, Anal. Chem. 83 (2011) 4004–4011, https://doi.org/10.1021/ac200616g.
[28] E.A. Vitol, Z. Orynbayeva, M.J. Bouchard, J. Azizkhan-Clifford, G. Friedman, Y. Gogotsi, In situ intracellular spectroscopy with surface enhanced Raman spectroscopy (SERS)-enabled nanopipettes, ACS Nano 3 (2009) 3529–3536, https://doi.org/10.1021/nn9010768.
[29] J.-F. Li, C.-Y. Li, R.F. Aroca, Plasmon-enhanced fluorescence spectroscopy, Chem. Soc. Rev. 46 (2017) 3962–3979, https://doi.org/10.1039/c7cs00169j.
[30] Y. Fu, J. Zhang, J.R. Lakowicz, Plasmon-enhanced fluorescence from single fluorophores end-linked to gold nanorods, J. Am. Chem. Soc. 132 (2010) 5540–5541, https://doi.org/10.1021/ja9096237.
[31] M.-X. Li, W. Zhao, G.-S. Qian, Q.-M. Feng, J.-J. Xu, H.-Y. Chen, Distance mediated electrochemiluminescence enhancement of CdS thin films induced by the plasmon coupling of gold nanoparticle dimers, Chem. Commun. 52 (2016) 14230–14233, https://doi.org/10.1039/c6cc08441a.
[32] Q. Chen, L. Liang, G. Potsi, P. Wan, J. Lu, T. Giousis, E. Thomou, D. Gournis, P. Rudolf, J. Ye, Highly conductive metallic state and strong spin–orbit interaction in annealed germanane, Nano Lett. 19 (2019) 1520–1526, https://doi.org/10.1021/acs.nanolett.8b04207.
[33] G. Marzari, M.V. Cappellari, G.M. Morales, F. Fungo, Electrochemiluminescent detection of glyphosate using electrodes modified with self-assembled monolayers, Anal. Methods 9 (2017) 2452–2457, https://doi.org/10.1039/c7ay00506g.
[34] V. Ayerdurai, M. Cieplak, K.R. Noworyta, M. Gajda, A. Ziminska, M. Sosnowska, J. Piechowska, P. Borowicz, W. Lisowski, S. Shao, F. D'Souza, W. Kutner, Electrochemical sensor for selective tyramine determination, amplified by a molecularly imprinted polymer film, Bioelectrochemistry 138 (2021), 107695, https://doi.org/10.1016/j.bioelechem.2020.107695.
[35] M.E. Draz, H.W. Darwish, I.A. Darwish, A.S. Saad, Solid-state potentiometric sensor for the rapid assay of the biologically active biogenic amine (tyramine) as a marker of food spoilage, Food Chem. 346 (2021), 128911, https://doi.org/10.1016/j.foodchem.2020.128911.
[36] J.B. Raoof, R. Ojani, M. Baghayeri, M. Amiri-Aref, Application of a glassy carbon electrode modified with functionalized multi-walled carbon nanotubes as a sensor device for simultaneous determination of acetaminophen and tyramine, Anal. Methods 4 (2012) 1579–1587, https://doi.org/10.1039/c2ay05494a.
[37] A. Küçük, O. Torul, Voltammetric sensor based on poly(3-methylthiophene) synthesized in dichloromethane for tyramine determination in moldy cheese, Synth. Met. 237 (2018) 23–28, https://doi.org/10.1016/j.synthmet.2018.01.009.
[38] D. An, Z. Chen, J. Zheng, S. Chen, L. Wang, Z. Huang, L. Weng, Determination of biogenic amines in oysters by capillary electrophoresis coupled with electrochemiluminescence, Food Chem. 168 (2015) 1–6, https://doi.org/10.1016/j.foodchem.2014.07.019.
[39] W. da Silva, M.E. Ghica, R.F. Ajayi, E.I. Iwuoha, C.M.A. Brett, Impedimetric sensor for tyramine based on gold nanoparticle doped-poly(8-anilino-1-naphthalene sulphonic acid) modified gold electrodes, Talanta 195 (2019) 604–612, https://doi.org/10.1016/j.talanta.2018.11.054.

Tamara Guerrero-Esteban obtained the Degree in Chemistry in 2016 from the Universidad Complutense de Madrid and the Master Degree in Quality and Food Safety in 2017 from the Universidad del País Vasco. She obtained her PhD Degree from Universidad Autónoma de Madrid in May 2023, in the Chemical Sensors and Biosensors group led by Prof. Encarnación Lorenzo. Her current research focuses on the development of electrochemiluminescent (bio)sensors for the detection of different analytes of interest.

Borja L. Sánchez earned a bachelor's degree in chemistry from Alcala de Henares University in 2021. During his final year, he had the opportunity of to study at Trinity College of Dublin through the Erasmus scholarship program. There, under the supervision of Jonathan Coleman, he focused on low-dimensional materials inks and their applications in printed electronics. In 2022, he completed a master's degree in Nanoscience and molecular Nanotechnology at Universidad Autonoma de Madrid. His master dissertation, supervised by Félix Zamora, involved researching on Covalent Organic Frameworks colloidal solutions. Subsequently, he began a Ph.D. in 2023 within the Nanomater group at Universidad Autonoma de Madrid by the supervision of Félix Zamora. He is current focus on bidimensional materials inks and their applications in various technologies.

Lucía Expósito Tribaldos obtained the Degree in Chemistry in 2022 from the Universidad Autónoma de Madrid. In her final project degree, she developed an electrochemiluminescent sensor for the detection of tyramine.

David Rodríguez-San-Miguel received his PhD in 2018. During it his interests were the development of new synthetic and processing methods of Covalent Organic Frameworks (COFs, a novel type of chemically tuneable porous materials) and the isolation of new 2D materials, namely antimonene. After successfully defending his PhD by the end of 2018, he joined the group of Dr. Puigmartí-Luis (part of the deMello group) at ETH Zürich as a postdoctoral researcher in January 2019. There, his research was focused on studying the synthesis of 2D COFs and MOFs in microfluidic conditions. In September 2020, with the appointment of Dr. Puigmartí-Luis as an ICREA Professor, he relocated with the Chem-InFlow group to Universitat de Barcelona. In 2021, he rejoined the group of Prof. Félix Zamora as a postdoctoral researcher, applying the acquired knowledge of microfluidics to the processing of COFs and 2D materials

Prof. Félix Zamora obtained his Ph.D. in Inorganic Chemistry at Universidad Autónoma de Madrid (1994), Spain. Then, he moved to the University of Dortmund (Germany) to

work with Professor B. Lippert. Félix is currently a Full Professor at the Inorganic Chemistry Department at the UAM. He is the author of over 233 manuscripts on chemistry and material science. In 2004 he focused his research on low-dimensional nanomaterials with electrical properties based on metal-organic and covalent organic frameworks (www.nanomater.es). He was awarded the Excellent in Research by BASF prize by the Spanish Royal Society in 2015 and appointed as a distinguished full professor with the mention of the Excellence Program for University Professors of the CAM in 2020.

Felix Pariente is currently Full Professor of Analytical Chemistry at the Universidad Autonoma de Madrid (UAM). He was born in Madrid in 1954. He received his B.S. and Ph. D. degrees in Chemistry in 1976 and 1988, respectively. Between 1992 and 1996 he spent several periods as visiting scientist at the University of Cornell in USA. In 1998 he obtains the degree of permanent assistant professor in the UAM. His research interest includes the design and development of enzyme biosensors and genosensors as well as processes involving electrocatalysis with application to the design of fuel cells and new analytical methods.

Cristina Gutierrez-Sánchez received her PhD degree from UNED in 2012. In the Bioelectrocatalysis laboratory of the Institute of Catalysis, CSIC, under the direction of Dr. Antonio Lopez De Lacey. She worked on the functionalization and characterization of surfaces using different techniques for the development of nanostructured enzyme electrodes. In 2013, she undertook her first postdoctoral contract at the University of Siegen, Germany. Subsequently, she moved to Marseille, France, to the CNRS Bioenergetics and Protein Engineering laboratory, for 2 years. Later, she joined the Bioelectrocatalysis group at the Institute of Catalysis, CSIC in 2016. At present, she is associate professor in the Department of Analytical Chemistry and Instrumental Analysis at UAM. Her main research interests include areas as Analytical Chemistry, Bioelectrochemistry, Nanoscience and Materials Science.

Encarnación Lorenzo is currently Full Professor in the Department of Analytical Chemistry and Instrumental Analysis at the Universidad Autonoma´de Madrid. She received her degree in Chemistry in 1978 and her PhD degree in 1985 from the Universidad Autonoma de Madrid. Afterwards, she made a post-doctoral stage at the Department of Chemistry at Dublin City University. In 1990 she was visiting scientist (NATO Program) to the Department of Chemistry in Cornell University. In 1998 the members of the faculty of Tokyo University of Agriculture and Technology invited her as visiting professor to the Department of Applied Chemistry. Actually, she is member of management committee of the Spanish Analytical Chemistry Society. Her research interest is the development of sensors and biosensors for the detection of analytes of environmental, clinical and food interest. She is the author/coauthor of more than 100 original research publications and several book chapters in the area of analytical chemistry